Structural and optical properties of Ce doped $BiFeO_3$ nanoparticles via sol–gel method

Jin Li ✉, *Xiao Ying Guan*

School of Physical Science & Technology, Xinjiang University, Urumqi 830046, Xinjiang, People's Republic of China
✉ *E-mail: xjlijin@163.com*

Published in Micro & Nano Letters; Received on 18th April 2019; Revised on 29th July 2019; Accepted on 4th September 2019

The effect of Ce doping on the structural and optical properties of $BiFeO_3$ nanoparticles via sol–gel method is reported. All samples were a pure phase with perovskite structure. The EDX results show the doped samples contain Bi, Fe, O and Ce elements. The vibrational properties of samples were studied using Raman spectroscopy. Photoluminescence shows an intense peak at 398 nm, the peak strength enhanced greatly and had redshift with the increase of Ce doping concentration. UV–vis results show the samples have a broad absorption band in the range of 500–600 nm. The bandgaps decrease with the concentration increase of Ce doping. It indicates the as-prepared $BiFeO_3$ can be used as visible light catalyst.

1. Introduction: Due to the wide applications in spintronic devices, modern optical, new information storage devices and sensors as well as the superior physical properties, bismuth ferrite ($BiFeO_3$) raise wide attention of scientific research workers [1–3]. $BiFeO_3$ shows a rhombohedral distorted perovskite structure and belongs to the R3c space group, which has lattice parameters, $a_r = 3.965$ Å and $\alpha_r = 89.43°$ at room temperature. $BiFeO_3$ material has very high ferroelectric Curie temperature (T_C ~830°C) and shows G-type antiferromagnetism Neel temperature (T_N ~370°C). It belongs to those few single-phase multiferroic materials which simultaneously possess ferroelectricity and antiferromagnetism at room temperature [4–6]. $BiFeO_3$ with smaller energy bandgap ($Eg = 2.3$–2.8 eV) also can be used as catalyst for the visible light [7]. However, the researches of optical property are less and lack of a comprehensive understanding.

Varied wet chemical methods have been applied to prepare $BiFeO_3$ nanostructures, such as hydrothermal route [8], conventional solid-state reaction [9, 10], ferrioxalate precursor method [11] and sol–gel technique [12–14]. Among these methods, the sol–gel method draws very attractively due to the easy control of chemical composition. On the other hand, it is well known that bi-site substitution with rare earth elements can reduce the leakage current of $BiFeO_3$. Considerable efforts have been reported by doping La [15–17]. And we know that cerium and lanthanum both belong to the lanthanides and the ionic radius of Ce (1.03 Å) is a little smaller than that of Bi (1.17 Å). Therefore, it is expected that Ce doping could reduce leakage current and induce structure distortions to improve the electrical properties of the $BiFeO_3$ materials [18].

In this Letter, we have focused on the synthesis of Ce doped $Bi_{1-x}Ce_xFeO_3$ ($x = 0$, 0.02, 0.04 and 0.06) nanoparticles by the sol–gel technique and we have investigated the effect of Ce and its concentration dependence on the structural, size and optical properties of $BiFeO_3$.

2. Experimental

2.1. Preparation of samples: $Bi_{1-x}Ce_xFeO_3$: ($x = 0$, 0.02, 0.04 and 0.06) nanoparticles were prepared by the sol–gel technique. The main chemical reagents used in the experiment are shown in Table 1. All the chemicals were analytical grade and were purchased from Shanghai Aladdin Biochemical Technology Co., Ltd (Shanghai, China).

Firstly, we prepared the 40 ml (0.25 mol/l) solution. 0.01 mol $Bi(NO_3)_3{\cdot}5H_2O$, 0.01 mol $Fe(NO_3)_3{\cdot}9H_2O$ and certain amounts of $Ce(NO_3)_3{\cdot}6H_2O$ (the molar ratio of $Ce(NO_3)_3{\cdot}6H_2O$ to Bi $(NO_3)_3{\cdot}5H_2O$ as 0, 2, 4 and 6%) were dissolved in 20 ml glacial acetic acid under constant magnetic stirring. Then, citric acid in 1:1 molar ratio with respect to the metal nitrates was added to the solution as a complexant. The mixture was stirred for about 30 min at 80°C, make samples dissolved absolutely, after being cooled to room temperature, measuring 20 ml glycol into the four groups of samples, respectively, continuously stirring at room temperature for 3 h to obtain the transparent, uniform and reddish-brown sol. Then, the sol was placed in a drying oven at 80°C until the clear sol was completely turned to the dried yellowish-brown gel and grounded into powders, the powders were preheated to 400°C at a ramp rate of 15°C/min for 1 h to remove the excess CH_x and NO_x impurities. Finally, the samples were annealed at 650°C in air for 2 h to get the $Bi_{1-x}Ce_xFeO_3$ ($x = 0$, 0.02, 0.04 and 0.06) nanoparticles.

2.2. Characterisation: X-ray diffraction (XRD, Philips X PPERT MPD) was used to measure the purity and crystalline structures of $Bi_{1-x}Ce_xFeO_3$ ($x = 0$, 0.02, 0.04 and 0.06) samples. The morphologies of $Bi_{1-x}Ce_xFeO_3$ nanoparticles were characterised by scanning electron microscope (SEM, LEO 1430VP), and the elemental compositions of the as-prepared samples were roughly estimated by energy-dispersive X-ray spectroscopy (EDX, M18XHF22-SRA) attached with the above SEM. The microstructural properties of as-synthesised samples were investigated by transmission electron microscopy (TEM, Hitachi H-600). The Raman spectrum (Raman, JY-HR800) give the lattice vibration characteristics of the samples. Fluorescent spectrophotometer (Fluorolog-3 21 TC SPC) was used to characterise the photoluminescence (PL) properties of $Bi_{1-x}Ce_xFeO_3$ samples. UV–vis absorption spectra of the samples were measured by UV–vis spectrophotometer (UV–vis, DRS, UV-2550) from 300 to 800 nm wavelength range.

3. Results and discussion: The XRD patterns of $Bi_{1-x}Ce_xFeO_3$ ($x = 0$, 0.02, 0.04 and 0.06) nanoparticles synthesised by the sol–gel method is shown in Fig. 1. It can be found that all the diffraction peaks (012), (104), (110), (006), (202), (024), (116) etc., are indexed to the distorted perovskite phase of $BiFeO_3$ (JCPDS Card No.71-2494, space group: R3c). The intense and sharp diffraction peaks imply the $BiFeO_3$ samples prepared are crystallised well. It also can be observed that very small amounts of Bi_2O_3 and $Bi_{25}FeO_{40}$ were present in the samples, a small amount of

Table 1 Main chemical reagents

No.	Name	Chemical formula	Molecular mass	Purity
1	bismuth nitrate	$Bi(NO_3)_3{\cdot}5H_2O$	485.07	AR (99.0%)
2	iron nitrate	$Fe(NO_3)_3{\cdot}9H_2O$	404.0	AR (98.5%)
3	cerium nitrate	$Ce(NO_3)_3{\cdot}6H_2O$	434.22	AR (99.95%)
4	ethylene glycol	$HOCH_2CH_2OH$	62.07	AR
5	citric acid	$C_6H_8O_7{\cdot}H_2O$	210.14	AR (≥99.5%)
6	glacial acetic acid	CH_3COOH	60.05	AR (≥99.5%)

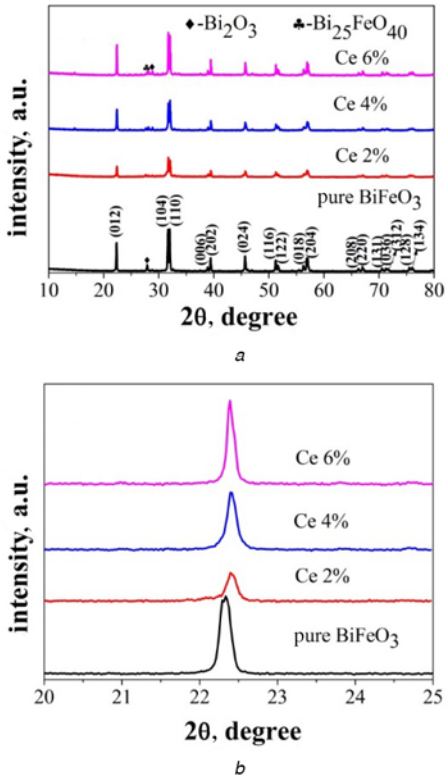

Fig. 1 *XRD patterns of $Bi_{1-x}Ce_xFeO_3$ ($x = 0$, 0.02, 0.04 and 0.06) nanoparticles*
a XRD patterns when 2θ from 10° to 80°
b Comparison of (012) diffraction peak positions to show the peak shift

impurities is hard to avoid in the process of sol–gel method. In addition, compared with the pure $BiFeO_3$, the diffraction peaks of $Bi_{1-x}Ce_xFeO_3$ ($x = 0.02$, 0.04 and 0.06) nanoparticles had a slight shift to big angle direction, which indicates the change of the lattice caused by the substitution of the Ce^{3+} ion. The shift of the diffraction peaks is considered as a result of the different radius of Bi^{3+} ion ($r = 1.17$ Å) and Ce^{3+} ion ($r = 1.03$ Å).

Figs. 2*a–d* show the SEM and EDX images of $Bi_{1-x}Ce_xFeO_3$ ($x = 0$, 0.02, 0.04 and 0.06, respectively) nanoparticles. The concentrations of Ce are calculated as $x = 0$, 0.02, 0.04 and 0.06, respectively. From these images, it can be seen that the pure $BiFeO_3$ powders are made up of irregular tiny particles and gathered denser. As observed from the images of doped samples, the doped samples also exhibited irregular and scattered. The EDX results show the doped samples contain Bi, Fe, O and Ce elements, while the Ce element cannot be found in the sample of $x = 0$. The actual atom content percentages of Ce are 0, 1.92, 3.75 and 5.94%, respectively. It can be concluded that Ce^{3+} ions were successfully doped into $BiFeO_3$ samples.

Figs. 3*a* and *b* show TEM images of the pure $BiFeO_3$ and $Bi_{0.9625}Ce_{0.0375}FeO_3$ nanoparticles, respectively. It is very clear that the pure $BiFeO_3$ particles are almost spherical in nature and agglomerated. The average particle size estimated about 150–200 nm. Compared with pure $BiFeO_3$ nanoparticles, the $Bi_{0.9625}Ce_{0.0375}FeO_3$ sample turns to decentralised spherical nanoparticles with the average size about 60 nm and distributes uniformly. The decrease in the crystal size can be attributed to the presence of Ce–O–Fe on the surface of the catalyst in the doped samples, which inhibits the growth of crystal grains.

Acting as a powerful tool, Raman spectroscopy can prospect the structural and vibrational properties of the materials. Fig. 4 shows the room temperature Raman spectra of the as-prepared pure $BiFeO_3$ and $Bi_{0.9625}Ce_{0.0375}FeO_3$ sample, with an excitation wavelength of 532 nm. For the $BiFeO_3$, it has a distorted rhombohedral perovskite structure belonging to the space group of R3c at room temperature. According to group theory, $BiFeO_3$ have 18 optical phonon vibration modes [19]:

$$\Gamma_{\text{opt.},R3c} = 4A_1 + 5A_2 + 9E$$

A_1 (TO) and E (LO) are Raman and infrared active vibration modes, respectively. And $5A_2$ is Raman inactive vibration mode, so $BiFeO_3$ have 13 Raman vibration modes [20]

$$\Gamma_{\text{Raman,R3c}} = 4A_1 + 9E$$

Among, A_1 and E are optical vibration modes, they can be divided into two modes: longitudinal optical (LO) mode and the transverse optical (TO) mode. We can know from Fig. 4, $BiFeO_3$ nanoparticles with ten Raman vibration modes, which is consistently well with the report by Zhiwu Chen earlier, all less than the theoretical value, it may due to Raman peak too weak or Raman peak overlap, etc. [21]. Stronger for three of the vibration frequency, A_1–1 A_1–2 and A_1–3 vibration modes, which appeared in the 136, 168, 219 cm^{-1}, and the relatively weak vibration mode A_1–4 is located at 452 cm^{-1}. In the rest of the 253, 277, 425, 364, 526 and 605 cm^{-1} belong to E vibration modes, were identified as E–2, E–3, E–4, E–5, E–6 and E–7, respectively. However, test wavenumber range does not include the E–1 mode at 75 cm^{-1}, we observed a small E mode at 277 cm^{-1}. Lattice vibration dynamic and transient information can be accurately recorded by Raman spectroscopy at the molecular level, so, Raman vibrational modes can reflect the influence of the Ce doping on the lattice structure with the change of doping amount. Compared with that of pure $BiFeO_3$ nanoparticles, E–2 and E–5 vibrational modes of the $Bi_{0.9625}Ce_{0.0375}FeO_3$ nanoparticles have the trend of wide, A_1–1, A_1–2 and A_1–3 vibration peak strength increases, the vibration frequency move to high frequency. These changes indicate that Ce^{3+} doped lead to Bi–O bond have changed in the samples.

Fig. 5 shows the photoluminescence (PL) emission spectra of $Bi_{1-x}Ce_xFeO_3$ ($x = 0$, 0.0192, 0.0375 and 0.0594) nanoparticles from 300 to 550 nm with a 245 nm excitation wavelength at room temperature. From Fig. 5, for the pure sample, it can be seen clearly a strong emission peak generated at 398 nm. For these doped samples, PL spectra have a slight red shift compared with the $BiFeO_3$ sample of $x = 0$ and the peak intensity increased greatly with Ce doping concentration. The intensity increase of the PL spectra with Ce^{3+} doping concentration pointed out the increase in the recombination of e− and h+. There are two large and asymmetric PL peaks seen from the inset of Fig. 5, demonstrate the existence of oxygen vacancy defects inside the energy bandgap, which is in accordance with the results reported by Moubah *et al.* [22]. Oxygen vacancy defects can be acted as the traps or recombination centres, which provide the carriers an alternative path to transfer energy and lead to the intense PL emission. The increase in the recombination of e− and h+ can be attributed to the increased amount of Ce that added up the oxygen vacancy defect sites

doi: 10.1049/mnl.2019.0236

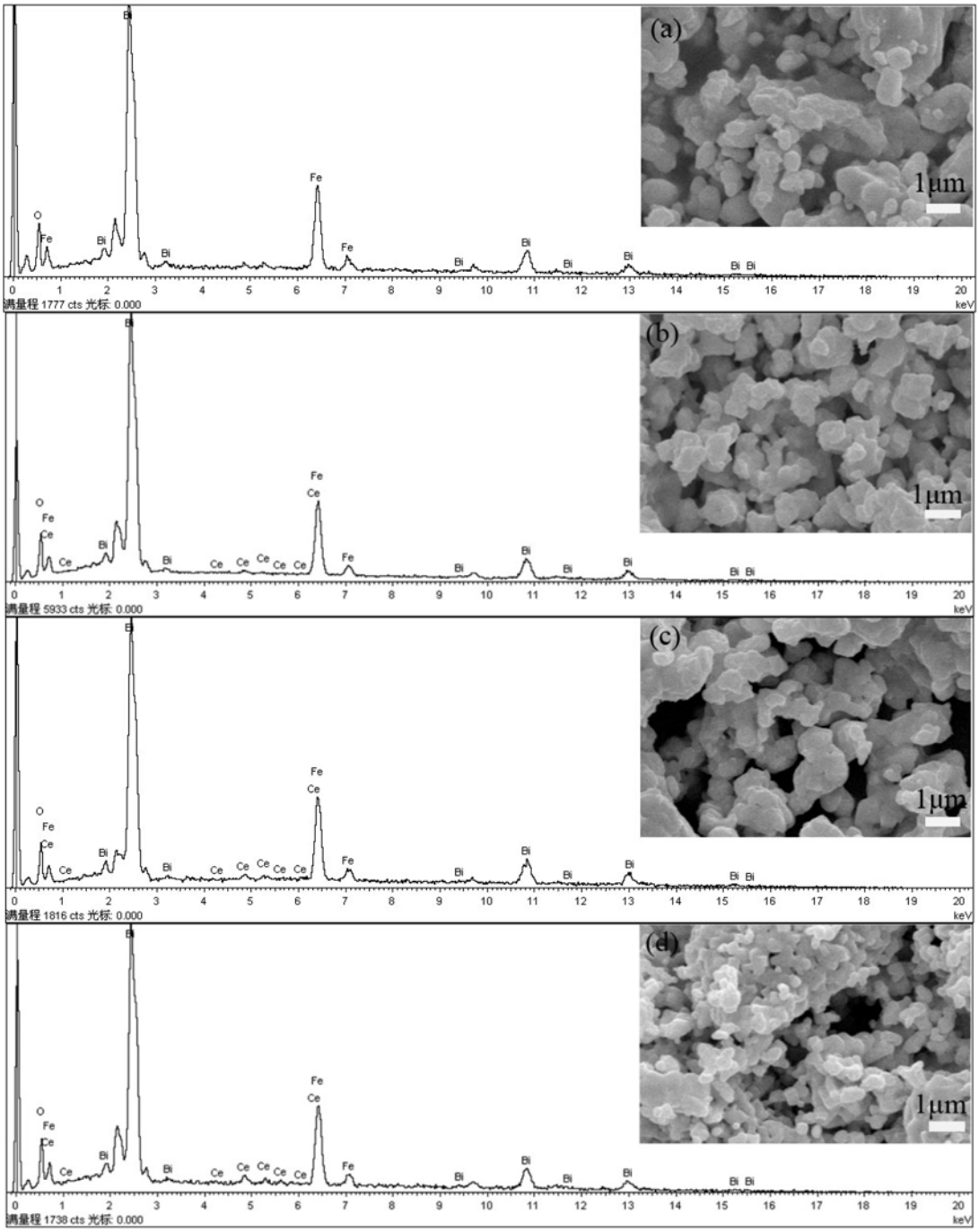

Fig. 2 *SEM and EDX patterns of $Bi_{1-x}Ce_xFeO_3$ nanoparticles*
a $x = 0$
b $x = 0.02$
c $x = 0.04$
d $x = 0.06$

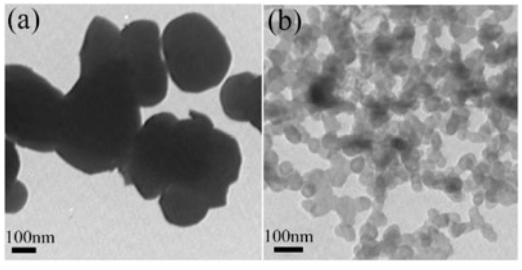

Fig. 3 *TEM images of samples*
a Pure $BiFeO_3$
b $Bi_{0.9625}Ce_{0.0375}FeO_3$

which behaved as the centres for the recombination of e− and h+ [23]. From the results of PL spectra, it can be known Ce-doped $BiFeO_3$ products have good luminescence properties in the visible wavelengths.

The UV–vis absorption spectrum patterns of $Bi_{1-x}Ce_xFeO_3$ ($x = 0$, 0.0192, 0.0375 and 0.0594) nanoparticles are shown in Fig. 6*a*. It can be observed that there are two absorption edges of all $BiFeO_3$ nanoparticles. The report presented the one absorption edge around 650 nm wavelength is because of metal-to-metal transition, while the other one about 750 nm results from the crystal-field transition [24]. The UV–vis absorption spectra of $Bi_{1-x}Ce_xFeO_3$ nanoparticles show as-prepared samples have a good visible light absorption indicating the materials can be used

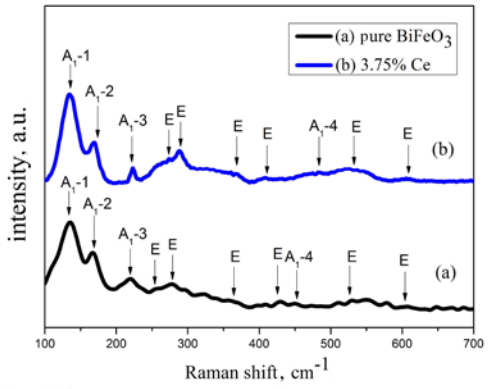

Fig. 4 *Room temperature Raman spectra*
a Pure $BiFeO_3$
b $Bi_{0.9625}Ce_{0.0375}FeO_3$ nanoparticles

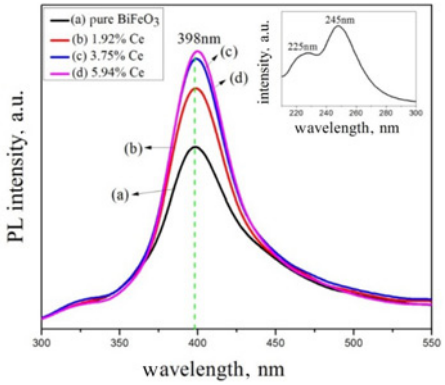

Fig. 5 *PL spectra of $Bi_{1-x}Ce_xFeO_3$ (x = 0, 0.0192, 0.0375 and 0.0594) nanoparticles at room temperature*

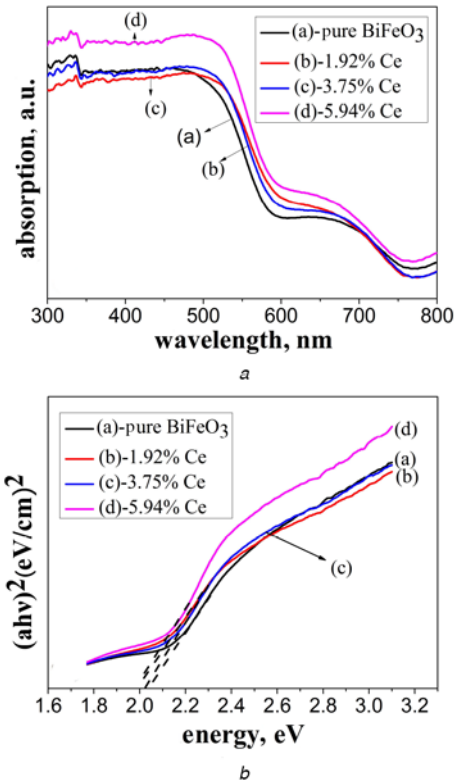

Fig. 6 *Optical properties of samples*
a UV–vis spectra of $Bi_{1-x}Ce_xFeO_3$ ($x = 0$, 0.0192, 0.0375 and 0.0594) nanoparticles at room temperature
b Plot of $(\alpha hv)^2$ versus photon energy (hv)

as a visible light photocatalyst for application. The energy bandgap (E_g) of $Bi_{1-x}Ce_xFeO_3$ nanoparticles has been estimated from the plot of $(\alpha hv)^{1/2}$ (α is absorption coefficient) versus photon energy (hv) shown in Fig. 6*b*. The intercept of the tangent to the X-axis gives well approximation to the energy bandgap of the as-prepared samples. When Ce was introduced into the samples, the slight red shift of absorption occurred, which indicated a decrease in the bandgap energy of these as-prepared samples. The estimated bandgap energies of all samples are 2.02, 2.01, 2.00, 1.97 eV, respectively. The bandgap of the pure $BiFeO_3$ is calculated as 2.02 eV, which is consistent with the report by Yang *et al.* [25]. The results implied as-prepared $Bi_{1-x}Ce_xFeO_3$ samples could be utilised in photocatalytic decomposition of organic contaminants under visible light irradiation.

4. Conclusions: In summary, Ce^{3+} ion doping $BiFeO_3$ nanoparticles were successfully synthesised using a sol–gel route. As-synthesised $BiFeO_3$ nanoparticles are rhombohedral distorted perovskite phase and belong to the R3c space group. The results of XRD indicate that pure phase $Bi_{1-x}Ce_xFeO_3$ crystallites could be obtained when Ce content is <6%. The results of SEM and EDX indicate that the doped samples contain Bi, Fe, O and Ce elements, and the particle size decreases with the concentration increase of Ce doping. The PL shows an intense electronic transition peak at a wavelength of 398 nm, and the peak strength enhanced greatly with the concentration increase of Ce doping. From UV–vis results, it can be known $BiFeO_3$ has a wide absorption band in the range of 500–600 nm wavelength range. The corresponding energy bandgap of the samples was calculated to decrease with the concentration increase of Ce doping. The results indicate the as-prepared $Bi_{1-x}Ce_xFeO_3$ nanoparticles have potential application as a visible light photocatalyst.

5. Acknowledgments: This work was financially supported by the National Natural Science Foundation of China (grant no. 11764040) and the College and University Scientific Research Plan Key Project of Xinjiang Uygur Autonomous Region (grant no. XJEDU2016I018).

6 References

[1] Gujar T.P., Shinde V.R., Kulkarni S.S., *ET AL.*: 'Room temperature electrodeposition and characterization of bismuth ferric oxide (BFO) thin films from aqueous nitrate bath', *Appl. Surf. Sci.*, 2006, **252**, pp. 3585–3590
[2] Basu S.R., Martin L.W., Chu Y.H., *ET AL.*: 'Photoconductivity in $BiFeO_3$ thin films', *Appl. Phys. Lett.*, 2008, **92**, p. 091905
[3] Wang C., Jin K., Xu Z., *ET AL.*: 'Switchable diode effect and ferroelectric resistive switching in epitaxial $BiFeO_3$ thin films', *Appl. Phys. Lett.*, 2011, **98**, p. 192901
[4] Folkman C.M., Baek S., Eom C.: 'Twin wall distortions through structural investigation of epitaxial $BiFeO_3$ thin films', *J. Mater. Res.*, 2011, **26**, (22), pp. 2844–2853
[5] Ramesh R., Spaldin N.A.: 'Multiferroics: progress and prospects in thin films', *Nature Mater.*, 2007, **6**, (1), pp. 21–29
[6] Wang J., Neaton J.B., Zheng H., *ET AL.*: 'Epitaxial $BiFeO_3$ multiferroic thin film heterostructures', *Science*, 2003, **299**, pp. 1719–1722
[7] Hao C., Wen F., Xiang J., *ET AL.*: 'Photocatalytic performances of $BiFeO_3$ particles with the average size in nanometer, submicrometer, and micrometer', *Mater. Res. Bull.*, 2014, **50**, pp. 369–373
[8] Chen X., Qiu Z., Zhou J., *ET AL.*: 'Large-scale growth and shape evolution of bismuth ferrite particles with a hydrothermal method', *Mater. Chem. Phys.*, 2011, **126**, (3), pp. 560–567
[9] Yao Y., Ploss B., Mak C.L., *ET AL.*: 'Pyroelectric properties of $BiFeO_3$ ceramics prepared by a modified solid-state-reaction method', *Appl. Phys. A*, 2010, **99**, (1), pp. 211–216
[10] Dai H.Y., Chen Z.P., Li T., *ET AL.*: 'Structural and electrical properties of bismuth ferrite ceramics sintered in different atmospheres', *J. Supercond. Novel Magn.*, 2013, **26**, (10), pp. 3125–3132
[11] Ghosh S., Dasgupta S., Sen A., *ET AL.*: 'Low temperature synthesis of bismuth ferrite nanoparticles by a ferrioxalate precursor method', *Mater. Res. Bull*, 2005, **40**, pp. 2073–2079

doi: 10.1049/mnl.2019.0236

[12] Kumar M., Yadav K.L., Varma G.D.: 'Large magnetization and weak polarization in sol–gel derived $BiFeO_3$ ceramics', *Mater. Lett.*, 2008, **62**, (8), pp. 1159–1161
[13] Gao T., Chen Z., Zhu Y., *ET AL.*: 'Synthesis of $BiFeO_3$ nanoparticles for the visible-light induced photocatalytic property', *Mater. Res. Bull.*, 2014, **59**, pp. 6–12
[14] Zhang H., Liu W.F., Wu P., *ET AL.*: 'Unusual magnetic behaviors and electrical properties of Nd-doped $BiFeO_3$ nanoparticles calcined at different temperatures', *J. Nanopart. Res.*, 2014, **16**, (1), pp. 1–9
[15] Lee D., Kim M.G., Ryu S., *ET AL.*: 'Epitaxially grown La-modified $BiFeO_3$ magnetoferroelectric thin films', *Appl. Phys. Lett.*, 2005, **86**, p. 222903-1-3
[16] Wang X., Liu H., Yan B.: 'Enhanced ferroelectric properties of Ce-substituted $BiFeO_3$ thin films prepared by sol–gel process', *J. Sol-Gel Sci. Technol.*, 2008, **47**, (2), pp. 124–127
[17] Liu J., Li M., Pei L., *ET AL.*: 'Effect of Ce doping on the microstructure and electrical properties of $biFeO_3$ thin films prepared by chemical solution deposition', *J. Phys. D, Appl. Phys.*, 2009, **42**, pp. 115409–115414
[18] Zhu X., Zhuge F., Li M., *ET AL.*: 'Microstructure dependence of leakage and resistive switching behaviours in Ce-doped $BiFeO_3$ thin films', *J. Phys. D, Appl. Phys.*, 2011, **44**, p. 415104
[19] Baettig P., Ederer C., Spaldin N.A.: 'First principles study of the multiferroics $BiFeO_3$, Bi_2FeCrO_6, and $BiCrO_3$: structure, polarization, and magnetic ordering temperature', *Phys. Rev. B*, 2005, **72**, (21), p. 214105
[20] Haumont R., Kreisel J., Bouvier P., *ET AL.*: 'Phonon anomalies and the ferroelectric phase transition in multiferroic $BiFeO_3$', *Phys. Rev. B*, 2006, **73**, (13), p. 132101
[21] Chen Z.W., Jin W.L., Lu Z.Y., *ET AL.*: 'Ferromagnetic and photocatalytic properties of pure $BiFeO_3$ powders synthesized by ethylene glycol assisted hydrothermal method', *J. Mater. Sci., Mater. Electron.*, 2015, **26**, (2), pp. 1077–1086
[22] Moubah R., Schmerber G., Rousseau O., *ET AL.*: 'Photoluminescence investigation of defects and optical band gap in multiferroic $BiFeO_3$ single crystals', *Appl. Phys. Express*, 2012, **5**, (3), p. 035802
[23] Nasir M., Xi Z., Xing M., *ET AL.*: 'Study of synergistic effect of Ce- and S-codoping on the enhancement of visible-light photocatalytic activity of TiO_2', *J. Phys. Chem. C*, 2013, **117**, pp. 9520–9528
[24] Tanabe Y., Sugano S.: 'On the absorption spectra of complex ions II', *J. Phys. Soc. Jpn.*, 1954, **9**, (5), pp. 766–779
[25] Yang X., Zhang Y., Xu G., *ET AL.*: 'Phase and morphology evolution of bismuth ferrites via hydrothermal reaction route', *Mater. Res. Bull.*, 2013, **48**, (4), pp. 1694–1699